SCIENTIFIC REPORTS

OPEN

Comparison of diffusion-weighted MRI and anti-Stokes Raman scattering (CARS) measurements of the inter-compartmental exchange-time of water in expression-controlled aquaporin-4 cells

Takayuki Obata [1], Jeff Kershaw[1], Yasuhiko Tachibana[1], Takayuki Miyauchi[2,3], Yoichiro Abe [2,3], Sayaka Shibata[4], Hiroshi Kawaguchi[5], Yoko Ikoma[1], Hiroyuki Takuwa[6], Ichio Aoki [4] & Masato Yasui[2,3]

We performed multi-b and multi-diffusion-time diffusion-weighted magnetic resonance imaging on aquaporin-4-expressing (AQ) and -non-expressing (noAQ) cells, and demonstrated a clear difference between the signals from the two cell types. The data were interpreted using a two-compartment (intra and extracellular spaces) model including inter-compartmental exchange. It was also assumed that restricted diffusion of water molecules inside the cells leads to the intracellular diffusion coefficient being inversely proportional to the diffusion-time. Estimates of the water-exchange-times obtained with this model are compared to those measured using an independent optical imaging technique (coherent anti-Stokes Raman scattering imaging, CARS). For both techniques it was found that the exchange-time estimated for the noAQ cells was significantly longer than that for the AQ cells.

Cell membrane water permeability (CMWP) is altered in diseases like cancer[1,2] and brain edema[3]. However, there is no medical imaging technique that can measure CMWP quantitatively. If such a technique were available for clinical use, it would prove very useful for disease diagnosis and therapy assessment.

An aquaporin (AQP) is a membrane channel protein that allows water molecules to be transported from one side of the membrane to the other. AQPs have been shown to regulate CMWP[4]. Recently, Ibata *et al.* reported a method to visualize water exchange between the intra- and extracellular spaces of AQP4 (a subtype of AQP) -expressing and -non-expressing cells using an optical imaging technique[5]. The technique they used is called coherent anti-Stokes Raman scattering (CARS) microscopy, which can selectively visualize H_2O. After quick replacement of the extracellular H_2O by D_2O, they succeeded in measuring the exchange-time of water from the intracellular to the extracellular space of a single HeLa S3 cell (100.7 ms for AQP4-non-expressing cells and 43.1 ms for AQP4-expressing cells). From those measurements they were able to quantify the difference in CMWP for the two cell types after estimating the water exchange-time and cell size. Although it may be difficult to apply this method to an *in vivo* study, information about the CMWP of each cell type may be extremely useful for *in vitro* validation of a potential clinical CMWP imaging method.

[1]Applied MRI Research, National Institute of Radiological Sciences, QST, Chiba, 263-8555, Japan. [2]Department of Pharmacology, Keio University School of medicine, Tokyo, 160-0016, Japan. [3]Keio Advanced Research Center for Water Biology and Medicine, Tokyo, 160-0016, Japan. [4]Department of Molecular Imaging and Theranostics, National Institute of Radiological Sciences, QST, Chiba, 263-8555, Japan. [5]Human Informatics Research Institute, National Institute of Advanced Industrial Science and Technology, Tsukuba, 305-8566, Japan. [6]Department of Functional Brain Imaging Research, National Institute of Radiological Sciences, QST, Chiba, 263-8555, Japan. Correspondence and requests for materials should be addressed to T.O. (email: obata.takayuki@qst.go.jp)
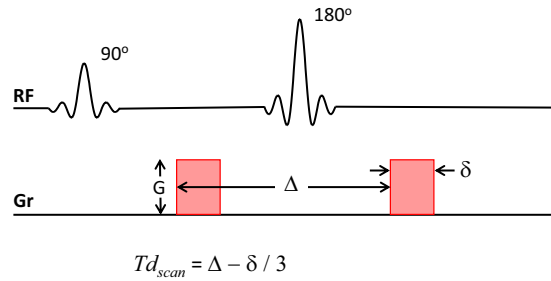
$$Td_{scan} = \Delta - \delta / 3$$

Figure 1. The PGSE sequence used to perform multi-b-value multi-Td (MbMTd) diffusion-weighted imaging (DWI). The sequence consists of 90° degree excitation and 180° refocusing RF pulses (RF) producing a spin echo, as well as magnetic field gradients (Gr) for diffusion weighting. The sequence diffusion-time (Td_{scan}) is calculated using the separation of the diffusion gradient lobes (Δ) and diffusion gradient duration (δ) ($Td_{scan} = \Delta - \delta/3$). The b-value is the product of Td_{scan} with the square of the spatial frequency (q), where $q = \gamma G \delta$ (γ, gyromagnetic ratio; G: gradient strength).

Diffusion-weighted magnetic resonance imaging (DWI) plays an important role in the diagnosis of diseases such as brain infarction and cancer[6]. Although it is understood that signal attenuation is due to the diffusion of water molecules, a reliable quantitative signal model relating tissue parameters and signal contrast remains to be established. CMWP must affect the DWI signal[7], but biological models used to interpret DWI usually treat the cell membrane as an impermeable wall[8–10]. One reason for this is that DWI is usually performed at diffusion-times (Tds) that are too short for the effect of CMWP on DWI signal to be easily observed. A second reason is that models that do account for CMWP are much more complicated. A third reason is that it is difficult to validate the measured quantitative CMWP value against a reliable standard. Several biological models that include cell permeability as a parameter of the system have been reported[11–15], but direct validation of the measurements is difficult.

In this study we performed multi-b-value multi-Td (MbMTd) DWI on AQP4-expressing (AQ) and -non-expressing (noAQ) Chinese hamster ovary (CHO) cells over a relatively wide range of Td, which was modulated by setting the separation of the diffusion gradient lobes (Δ) to 40, 70, or 100 ms to change the sequence parameter Td_{scan} (Fig. 1). We also applied a simple DWI signal model that enabled us to estimate the exchange-time of water between the intra- and the extracellular spaces. The results were then compared with the results of the CARS experiments[5].

Theory

Water exchange-time measurement with MRI. The Kärger model[15–17], which is a simple two-compartment model with inter-compartmental compound exchange, was used as a base model for analysis ("Original" in Fig. 2). The model assumes free Gaussian diffusion of water in each compartment (ie D_{ex} and D_{in} are constant), but many papers indicate that *in vivo* water diffusion is non-Gaussian[18,19]. We modified the model ("Modified" in Fig. 2) under the assumption that Td_{scan} is sufficiently long that the diffusion coefficient in the extracellular space (D_{ex}) is approximately constant, while that in the intracellular space (D_{in}) is inversely proportional to the diffusion-time (see Discussion and Methods sections)[18]. The data was then analyzed using Td-independent D_{ex} and Td-dependent D_{in} as below,

$$D_{in} = \frac{\alpha}{Td_{scan}^{\beta}}, \tag{1}$$

where α has dimensions of length squared in the case that $\beta = 1$, while β is a parameter inserted to test the assumption that D_{in} is inversely proportional to Td_{scan} ("Modified" in Fig. 2).

Using the modified model, the MRI-based estimate of the exchange-time (τ_{MRI}) is[14],

$$\tau_{MRI} = F_{ex} \cdot t_{in} = F_{in} \cdot t_{ex}, \tag{2}$$

where F_{ex} and F_{in} are the signal fractions of the extracellular and intracellular spaces, respectively, and t_{ex} and t_{in} are the lifetimes in the extracellular and intracellular spaces, respectively. Note that $F_{ex} + F_{in} = 1$.

Water exchange-time measurement with CARS. The water exchange-times between the intracellular and extracellular spaces were also investigated with CARS microscopy. Ultra-high-speed line-scan CARS images were obtained every 0.488 ms. This technique can discriminate between H2O and D2O signal, as well as allow selective imaging of the extracellular and intracellular spaces. After rapid replacement of H2O with D2O in the extracellular space (replacement time is less than 20 ms), the intracellular H2O signal was observed. Details of the experiment can be found in the previous report by Ibata et al.[5]. The CARS-based estimate of the exchange-time (τ_{CARS}) is calculated with

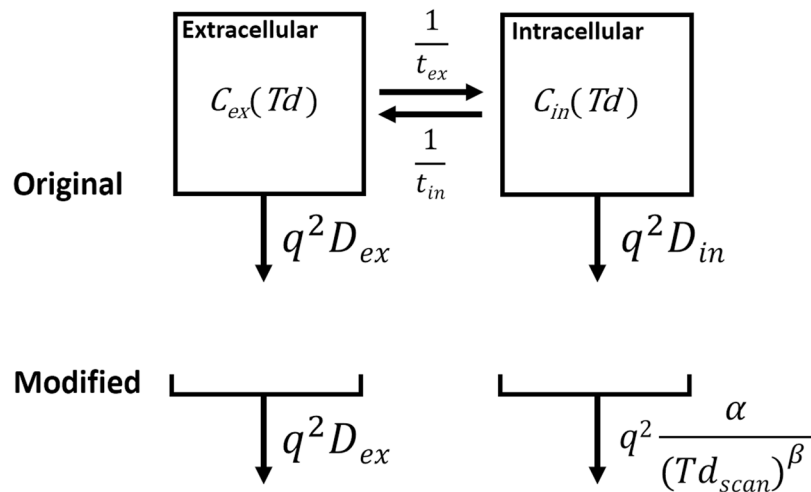$$S_{in}(t) = A e^{-\frac{t}{\tau_{CARS}}} + B \tag{3}$$

2

Figure 2. Two-compartment models including inter-compartmental exchange. $C_{ex}(Td)$ and $C_{in}(Td)$ are the normalized extracellular and intracellular signals, respectively, at diffusion-time Td. t_{ex} and t_{in} are constants representing the inter-compartmental lifetimes. D_{ex} and D_{in} are the diffusion coefficients in the extracellular and intracellular spaces, respectively. The water signal from each compartment decreases with a rate constant, $q^2 D$. In the original Kärger model (top), D_{ex} and D_{in} are both constant and Td-independent, while for the modified model (bottom) D_{ex} is constant, and D_{in} is modelled as "$\alpha/(Td_{scan})^\beta$", where Td_{scan} is the experimental diffusion-time, "β" is a parameter to test our assumption that D_{in} is inversely proportional to Td_{scan}, and "α" is a fitting parameter with units of length squared if $\beta = 1$. "q" is the q-value determined by the parameters of the motion probing gradient.
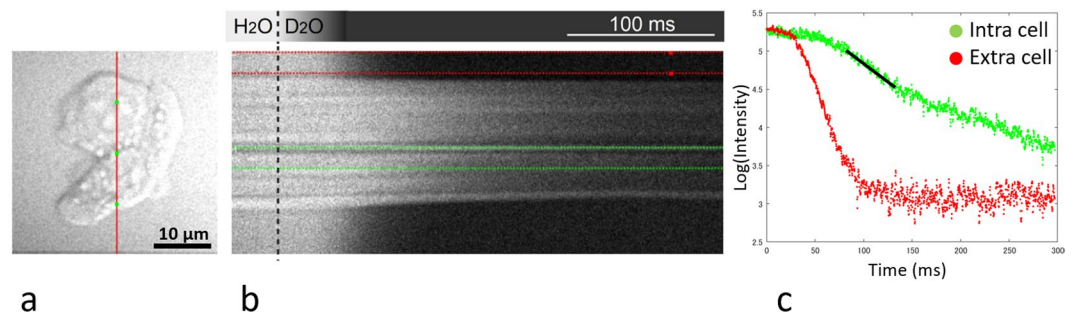

Figure 3. Coherent anti-Stokes Raman scattering (CARS) microscopy. This technique can selectively visualize H_2O (**a**). After rapid replacement of H_2O with D_2O (no signal) in the extracellular space, water exchange between intracellular and extracellular space can be observed (**b**) using line scans taken where the red line in (**a**) is drawn. (**c**) is a logarithmic graph of the time-intensity curves for the intracellular (green dots) and extracellular (red dots) spaces. The plotted intensity is the mean value between the green or red colored lines in (**b**). Regression over a range of 50 ms was performed where the slope in (**c**) appears steepest (black line) on the logarithmic graph of the time-intensity curve, and the inverse of the slope from the fit was taken as the estimate of τ_{CARS}.

where $S_{in}(t)$ is the signal intensity from inside a single cell, and A and B are constants. Regression over a range of 50 ms was performed where the slope appears steepest on a logarithmic graph of the time-intensity curve, and the inverse of the slope from the fit was taken as the estimate of τ_{CARS} (Fig. 3c).

Results

Multi-b-value multi-*Td* (MbMTd) DWI.   As measured by an automated cell counter the survival rate of both the noAQ and AQ cells after MRI examination was more than 97%, and the radius of both cell types was in the range of 6.0–7.1 μm.

Separate apparent diffusion coefficient (ADC) maps were calculated for the images with b = 0–1500 s/mm² (low b) and b = 4000–8000 s/mm² (high b) ranges using single-exponential fitting to the data acquired with $\Delta = 100$ ms (Fig. 4). The low-b range ADC map appeared to depend on depth, while the high-b range ADC map was more sensitive to differences in AQP4 expression. The mean b-value dependent signal changes from ROIs drawn midway down the cell cultures were compared in Fig. 5. The data were normalized by measurements made with b = 0. For the data measured at $\Delta = 40$ ms, the noAQ signal was similar to the AQ signal across the full range of b values. At $\Delta = 70$ ms both the noAQ and AQ signals decayed more slowly with b-value than at $\Delta = 40$ ms. However, as the attenuation for noAQ was slower, there was a clear difference between the noAQ and AQ signals.
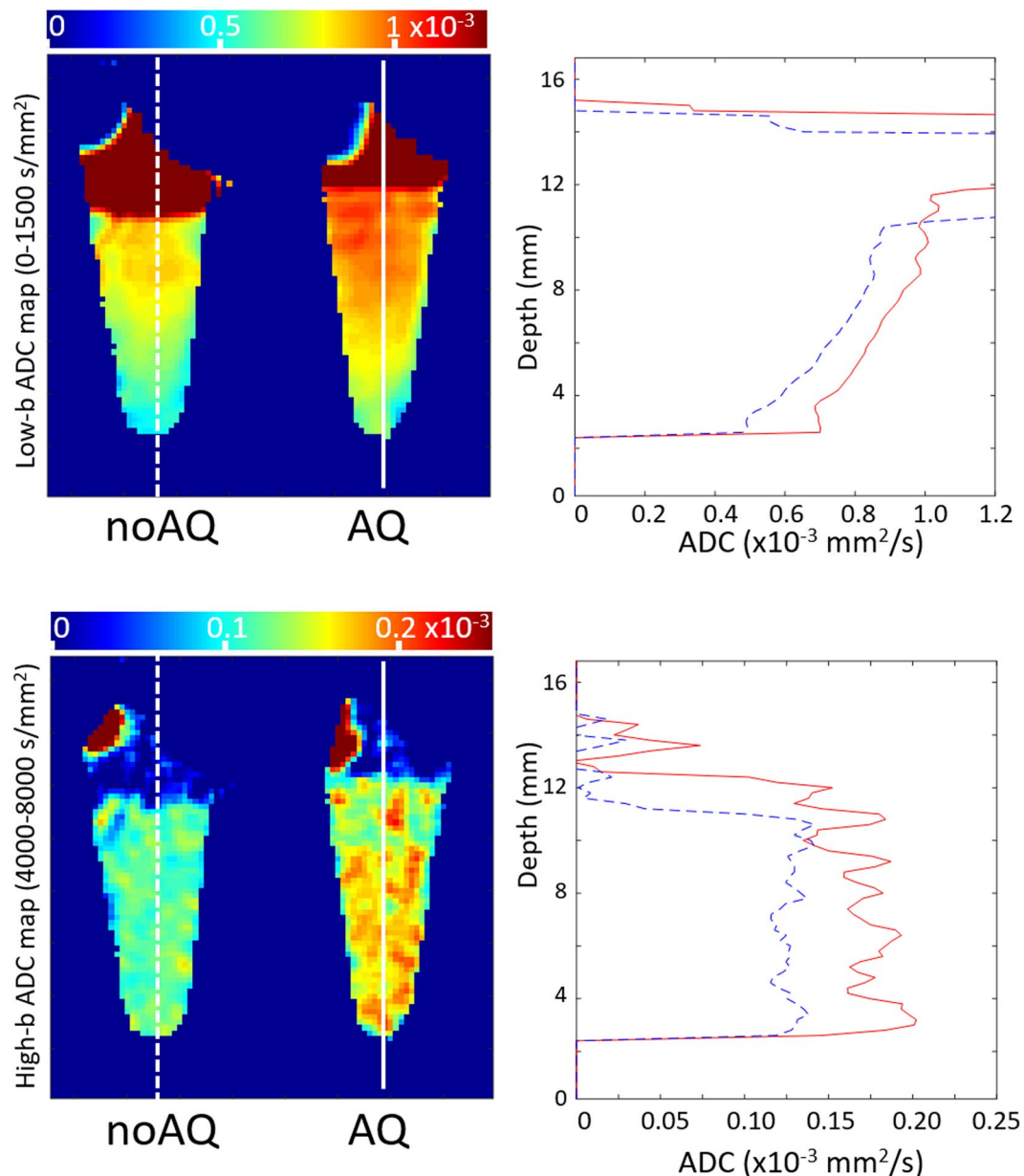
Figure 4. Profiles along lines drawn on ADC maps ($\times 10^{-3}$ mm²/s) of aquaporin-4-expressing (AQ, solid lines) and -non-expressing cells (noAQ, dashed lines) in PCR tubes. The ADC maps were calculated from the $\Delta = 100$ ms data, with the low-b and high-b ranges corresponding to b $= 0$–1500 s/mm² and b $= 4000$–8000 s/mm², respectively. The low-b ADC appears to depend on the depth within the sample tube, while the high-b ADC may be more sensitive to AQP4 expression.

The difference between noAQ and AQ was further enhanced as Δ was increased to 100 ms. The noAQ signal at $\Delta = 100$ ms was similar to that at $\Delta = 70$ ms, but that of AQ was slightly reduced from $\Delta = 70$ ms to 100 ms, which is the primary source of the enhancement (Fig. 6).

Model fitting. After fitting the data to the proposed model ("Modified" in Fig. 2), it was found that the fitted curves are consistent with the observed data across all Δs (Fig. 6). The estimates of τ_{MRI} for the noAQ and AQ cells were 55.1 ± 5.0 ms and 39.2 ± 10.3 ms, respectively (Fig. 7), and there was a significant difference between these two values (unpaired-t test, p $= 0.0016$). There was also a significant difference in the estimates of t_{in} for the two cell types (unpaired-t test, p < 0.0001). Other parameter estimates had no significant differences. The parameters α and β for the intracellular diffusion were $6.26 \pm 0.10 \, \mu m^2$ and 0.955 ± 0.016 for noAQ, and $6.49 \pm 0.44 \, \mu m^2$ and 0.968 ± 0.014 for AQ, respectively. All parameter estimates are summarized in Table 1.

The exchange-time for individual cells of each cell type were also measured with the CARS technique (τ_{CARS}). There was a clear significant difference in τ_{CARS} between the noAQ (152 ± 33) and AQ cells (87.7 ± 22.9 ms) (unpaired-t test, p $= 0.0002$, Fig. 7).
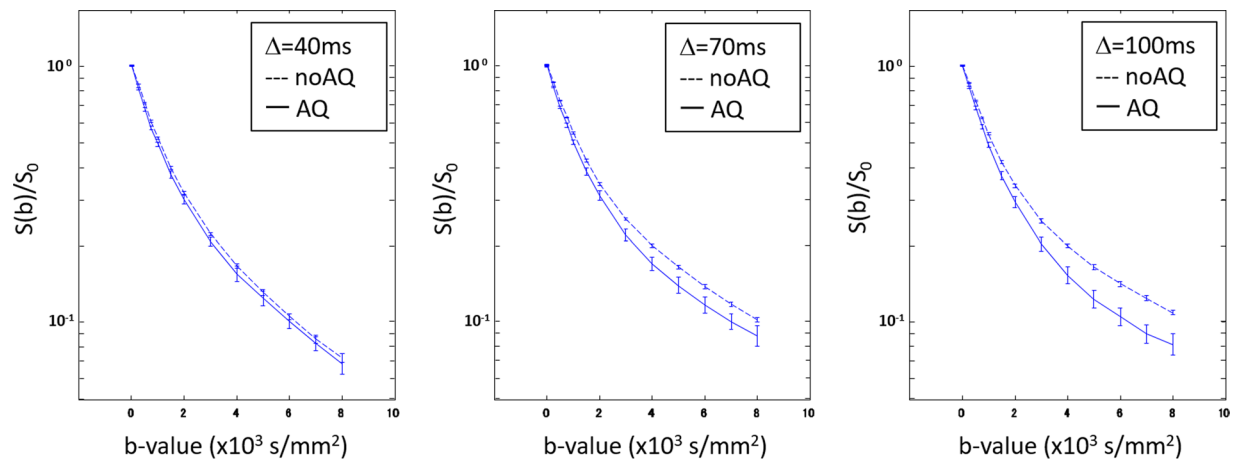
Figure 5. Normalized b-value-dependent signal decay for the noAQ and AQ samples at different diffusion-times. Separation between the curves of the two cell types increases with diffusion-time. Also of note is that the AQ signal at high b-value increases from $\Delta = 40$ ms to 70 ms, but decreases from $\Delta = 70$ ms to 100 ms. This behavior cannot be explained by a simple Gaussian or restricted diffusion model.
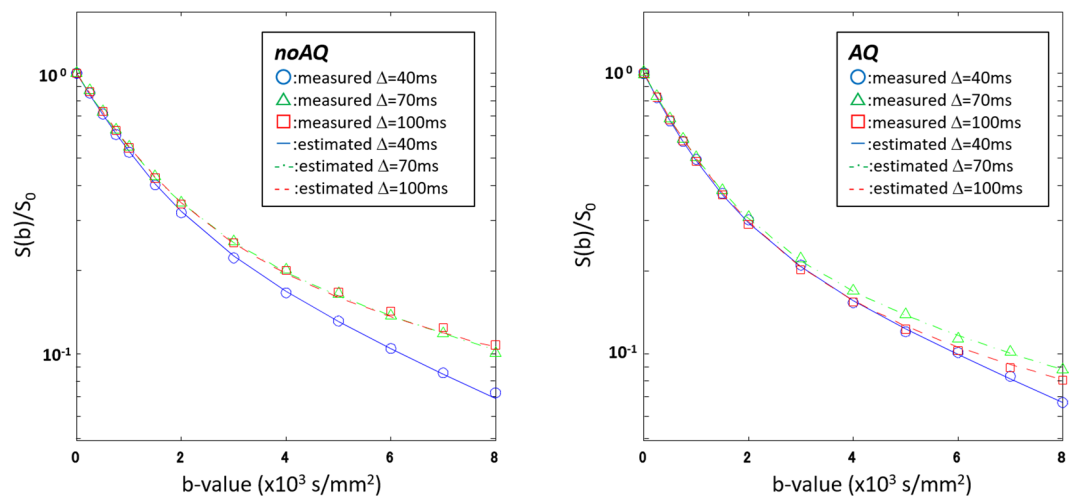

Figure 6. Curve fits using the proposed model. The graphs present fits to Eqs 7–9 for both the noAQ (left) and AQ (right) data using the proposed functional form: $D_{in} = \alpha / Td_{scan}{}^{\beta}$ ("Modified" in Fig. 2). The fitted curves are consistent with the observed data for all Tds. All parameter estimates for the model are summarized in Table 1.

	t_{in}(ms)	t_{ex}(ms)	F_{in}	$D_{ex}(\times 10^{-3}\,mm^2/s)$	α	β
noAQ	89.5 ± 5.4*	144 ± 21	0.385 ± 0.029	1.18 ± 0.08	6.26 ± 0.10	0.955 ± 0.016
AQ	61.1 ± 12.3*	112 ± 42	0.365 ± 0.044	1.35 ± 0.25	6.49 ± 0.44	0.968 ± 0.014

Table 1. Estimates of the parameters for the "modified" two-compartment model with inter-compartmental exchange. t_{in} and t_{ex}, lifetimes in the intra- and extracellular spaces, respectively; F_{in}, signal fraction from intracellular space; D_{ex}, apparent diffusion coefficient for the extracellular space; α and β, parameters for the functional form $D_{in} = \alpha / Td_{scan}{}^{\beta}$ for "Modified" in Fig. 2. * indicates a significant difference between the AQ and noAQ estimates (unpaired-t, p < 0.0001).

Discussion

Multi-b-value multi-*Td* (MbMTd) DWI. In this study, the low-b ADC map appears to depend on the depth within the samples, while the high-b ADC is more sensitive to depth-independent factors such as AQP4 expression (Fig. 4). It has been argued in a previous study that for the low-b value range, ADC mainly reflects the balance between extracellular and intracellular volume fractions[20], which may be the main reason why the low-b ADC is more depth-dependent. The intracellular fraction of both cell types is expected to be larger at greater depth because deep cells are more densely packed after being centrifuged. On the other hand, at high b-value the signal may be more heavily weighted by the intracellular contribution because the motion of extracellular
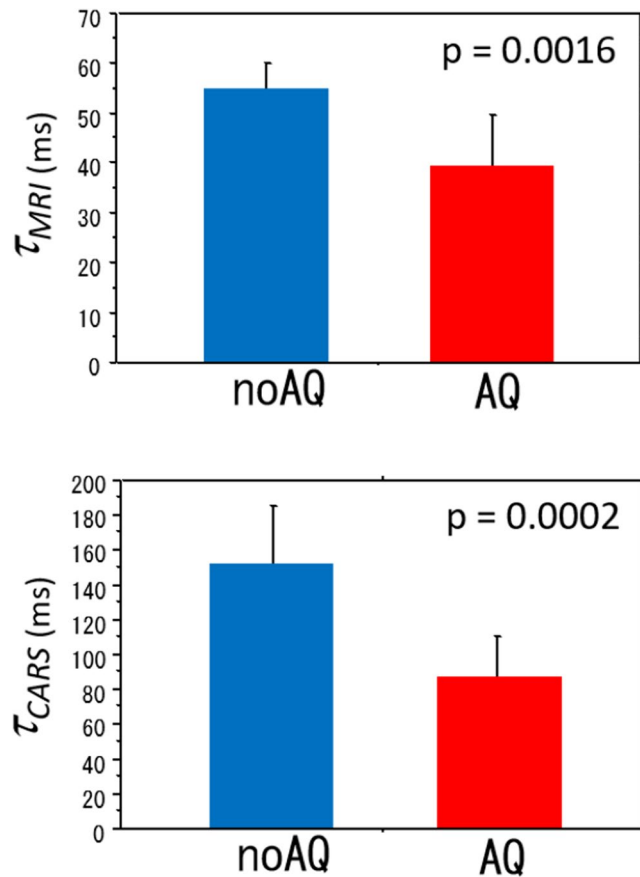
Figure 7. Exchange-times for AQP4-non-expressing (noAQ) and expressing (AQ) cells measured with MRI (τ_{MRI}) and CARS (τ_{CARS}). Both τ_{MRI} and τ_{CARS} for noAQ are longer than those for AQ. There are significant differences in both exchange-times between noAQ and AQ.

molecules is less restricted, and therefore the extracellular signal is more strongly attenuated with higher b-value than intracellular signal (extracellular signal at b = 4000 s/mm² is less than 5% of the total signal)[21]. In this case it is likely that the remaining signal reflects factors that influence the diffusion of intracellular water molecules. Among these factors, the major physical difference between the two cell types is the AQP4 expression, which suggests that the different ADCs of the cell types at high b-value is related to CMWP.

Model fitting. In this study we found a difference in the b-value-dependence of the normalized signal changes between noAQ and AQ cells. The difference in the signal was more noticeable at higher b-value and longer Td. The results are consistent with the concept that water has more time to exchange between extra- and intracellular spaces at longer Td. Therefore, we proposed a suitable model with which CMWP can be estimated from the Td-dependent signal changes.

As mentioned in the Theory section, the simplest model for DWI signal attenuation that includes inter-compartmental exchange is that reported by Andrasko and Kärger (Original in Fig. 2)[15–17]. This model assumes free Gaussian diffusion of water, in which case the diffusion coefficient of the water is independent of Td. Under this model, if the water exchange is zero, then the b-value-dependent signal decay curves should be similar for all Tds. In contrast, if the inter-compartmental water exchange is nonzero, the normalized b-value-dependent signal should decay faster at longer Td. However, the signal decay for both the noAQ and AQ cells at $\Delta = 70$ ms was slower than that at $\Delta = 40$ ms (Fig. 5), which means that the results are not consistent with this model. Fieremans *et al.* also suggested that the original Kärger model overestimates the exchange-time for cells with high permeability[14].

As the original Kärger model is not suitable for describing *in vivo* water diffusion, we modified the model with consideration of the nature of intracellular diffusion. It has been suggested that intracellular diffusion might be roughly modeled as restricted diffusion inside a sphere of diameter A[22]. In that case, for long diffusion-times ($Td \gg A^2/2D$; D is the free-water diffusion coefficient), the apparent diffusion coefficient is approximately inversely proportional to Td. Hence, the functional form adopted for D_{in} in Eq. 1. For the case of extracellular water diffusion, even though water molecules are hindered by the cell membrane to some extent, they may still travel very large distances in comparison to the cell dimension[8]. According to previous studies, the Tds used in the present work (37.7, 67.7, and 97.7 ms) are long enough to treat the observed D_{ex}s as Td-independent[9,10,23,24]. Our previous work was also consistent with those reports (Supplementary Fig. S1)[25]. In accordance with these ideas, we analyzed the data using a Td-independent D_{ex} and the functional form $\alpha/Td_{scan}{}^\beta$ for D_{in} (Modified in Fig. 2). As mentioned

in the theory section, the parameter α has the dimensions of length squared in the case that $\beta = 1$, while β is a parameter inserted to test the assumption that D_{in} is inversely proportional to Td_{scan}. The curve fitting matched the data well as shown in the Results section. In this fitting, the values of β were near 1 (0.955 ± 0.016 for noAQ, and 0.968 ± 0.014 for AQ), which is consistent with our assumption for the model. If β is equal to 1, α should be $A^2/5$[18], and the radii of the noAQ and AQ cells can be estimated as 5.7 and 5.8 μm, respectively. These values are consistent with those obtained from direct measurement (6–7.1 μm). Overall, our model works well for the analyses of DWI for the noAQ and AQ cell samples.

Discrepancy in the exchange-times measured with MRI and CARS. Both τ_{MRI} and τ_{CARS} were longer for the noAQ cells, however, the former (88.9 ms for noAQ and 62.7 ms for AQ) are lower than those of the latter (152 ms for noAQ and 87.7 ms for AQ). There are a number of possible reasons for this. First, MRI does not visualize all water protons because some protons (e.g. bound water protons) have a T2 that is too short. Such water protons may have very long exchange-time. It follows that τ_{MRI} may be shorter than the exchange-time for all water molecules that is measured by CARS. Second, the replacement of extracellular H_2O with D_2O in the CARS experiment was very quick, but the exchange-time is nonzero (≈ 16.1 ms[5]). This exchange-time should be considered when assessing the true exchange-time. The difference in the exchange-time between MRI and CARS measurements for the AQ cells is small enough that it might be compensated in this way. However, the difference between τ_{MRI} and τ_{CARS} for noAQ cells is too large to be explained by this mechanism. Third, the range of the Td (37.7–97.7 ms) may be too low for accurate calculation of the exchange-time for noAQ cells. The CARS estimate of the intracellular water exchange-time for noAQ cells was 152 ms. Ideally, measurements should be performed over a diffusion-time range that includes this value. Fourth, even though the room temperature was kept at 22 C during experiment, it is possible that the temperature in the PCR tube increased due to RF and magnetic gradient switching. Ibata *et al.* reported that intracellular water exchange-time is shorter at higher temperature, and this is especially true for the noAQ cells[5]. Such a temperature difference may produce a large difference in the water exchange-time measured for noAQ cells with MRI and CARS. Finally, the difference in cell density between the samples used for MRI and CARS measurements may affect the results of the measured exchange-times. The cells were packed tight in the MRI sample, while the density was much lower in the CARS sample.

Although a difference in τ_{MRI} between the noAQ and AQ cells was successfully observed with our MRI technique, the quantitative values produced by the method still need to be validated in further studies. Similar experiments were performed by Thelwall *et al.* using human erythrocyte ghosts[11]. The reported exchange-time (20–24 ms) is smaller than those we obtained. The main reason for the difference with our measurements may be the difference in cell volumes; cells with the same permeability but larger volume will have longer exchange-time. Differences in the temperature condition during the performance of the experiments is another possible reason for the difference[12].

Potential of this method for human application. It is often difficult to observe Td-dependent ADC changes in normal tissue, but some reports suggest that pathological tissue, such as in the case of cancer[26] and stroke[27], may show characteristically large signal changes in DWI when Td is changed. Many clinical researchers are therefore interested in multi-Td measurements.

One advantage of our method is that it can easily be applied in clinical examinations. Since the Td_{scan}s are relatively long, the magnetic gradient amplitude necessary to create high b-values is not too strong even for clinical systems. One difficulty is that a relatively long TE has to be used to achieve the long Td_{scan}s, and consequently the signal-to-noise ratio (SNR) is lower than for usual clinical DWI. However, since the main targets of permeability measurement are white matter dysfunction and cancer, which have low ADCs, sufficient SNR will be available in those areas even when using long TE. Reports of the exchange-times in highly-permeable lesions, such as brain infarction and viable cancer, suggest that the diffusion-times available to our spin-echo method are sufficient for reliable quantitative measurements[5,27,28]. A stimulated-echo sequence (STE) is another possible way to lengthen Td[29], although the SNR is only about 50% of spin-echo imaging. It should be remembered, however, that the longer mixing time (time between the 2nd and 3rd 90 degree pulses) required for longer Td may change T1-related signal contrast in STE DWI.

A survey of the literature finds that non-invasive clinical CMWP measurement has not yet been established. Although clinical MR scanners have more limitations than animal ones, clinical application of our method may provide new information concerning cell characteristics. Ozarslan *et al.* reported the diagnostic potential of diffusion-time-dependent MR signal changes[30]. AQP4 is known to express on the membrane of the endfeet of astrocytes, where it regulates permeability. Some reports have suggested that AQP4 expression affects the severity of brain infarction[2]. Measurement of AQP4 antibodies is used for clinical diagnosis of neuromyelitis optica (NMO), which may also be related to the function of AQP. Other types of aquaporin are also involved in diseases such as cancer, nephrogenic diabetes insipidus, and cataracts[31–33]. Therefore, the proposed method may be useful for the diagnosis of disease and therapy assessment.

Limitations
A limitation of the model used in this paper is that it does not account for possible differences between intracellular and extracellular T1 & T2. Significant differences between the intracellular and extracellular relaxation times could lead to systematic errors in the parameter estimates, which could also be another source of discrepancy between the exchange-times measured with MRI and CARS. Several studies on intracellular and extracellular relaxation times have been published[34–36]. Proton relaxation in a biological environment is complicated; it involves cross-relaxation and chemical-exchange between protein and bound and free water protons, as well as water exchange between intra- and extracellular compartments. Nevertheless, there is no well-established model

for intercompartment water exchange that includes both diffusion and T1 & T2 relaxation effects[13,27,37,38]. The possible influence of T1 and T2 relaxation should be considered more closely in future research.

Another possible limitation of the model is that it does not consider anisotropy of water diffusion, so it cannot simply be applied to water diffusion in white matter. Myelinated neuron fibers have such a small permeability that impermeable anisotropic models may be more useful[8,9]. Additionally, it should be noted that DWI at high-b values has a low signal-to-noise ratio, which means that the data should be analyzed carefully[39,40]. The noise signal floor in the experiments was at most 1% of the signal in the b = 0 images, which is much lower than the signal for the highest b-value.

Conclusion

In conclusion, we performed multi-b and multi-diffusion-time DWI on AQP4-expressing and -non-expressing cells, and demonstrated a clear difference between the signals from the two cell types. The data were interpreted with a two-compartment model including inter-compartmental exchange, and this was used to estimate the water-exchange-time, which was consistent with one-cell measurement data obtained with CARS. The results indicate that this method might be used to characterize cell-membrane water permeability.

Methods

Cell culture and transfection.
The cellular experiments in this study were performed in accordance with our local guidelines.

Chinese hamster ovary (CHO) cells stably transfected with either the expression vector pIRES2-EGFP, in which a unique AflII site had been modified to an EcoRI by linker ligation containing mAQP4 M1 cDNA (AQ), or the empty vector (noAQ) were maintained in Ham's F-12 (Wako, Japan) supplemented with 10% FBS (fetal bovine serum) (Sigma), 1% penicillin/streptomycin (Life Technologies) and 0.5 mg/mL G418 antibiotics (Nacalai tesque) in 10-cm culture dishes at 37 °C in a humidified atmosphere (5% CO_2–95% air). Stable CHO-cell clones were established as described in previous studies[41,42]. In brief, the plasmids were linearized with EcoRI and transfected into CHO cells with Lipofectamine and Plus reagents (Life Technologies). Forty-eight hours after transfection, cells were re-seeded onto ten 10-cm dishes and selected for ten days with G418. Several colonies showing green fluorescence were picked up and amplified.

Cell suspensions.
The cells were centrifuged at 800 rpm for 5 min at 4 °C. A suspension of 0.2 ml containing 2.5×10^7 cells was prepared with PBS in a PCR tube (0.5 ml in size) for each cell type. Room temperature was maintained at 23 °C. A sample was extracted from each cell suspension prior to MR acquisition, and another was extracted after MR acquisition to detect possible changes over time. All samples were photographed using an inverted light microscope at a magnification of ×200. The percentages of cell survival were calculated with trypan blue, and the mean and the range of cell size was calculated from each photograph by an automated cell counter (Invitrogen Countess, Thermo Fisher Scientific, Japan).

MRI acquisition.
A 7T animal MRI (Kobelco with Bruker BioSpin, Japan) with a volume resonator for transmission (Bruker Biospin, Germany) and a quadrature surface coil for reception (mouse brain coil, Rapid biomedical, Germany) was used for this experiment. The two cell samples (noAQ and AQ) were set in the gantry on a PCR tube holder (homemade) together with a PBS sample as a reference. The temperature of the air around the sample was maintained at approximately 22 °C.

Multi-b-value multi-Td (MbMTd) DWI was obtained using a pulsed-gradient spin-echo (PGSE) sequence with four-shot EPI acquisition (TR = 3 s, TE = 115 ms, matrix size = 128 × 128, spatial resolution = 0.02 × 0.02 mm², slice thickness = 2 mm). The separation of the diffusion-gradient lobes (Δ) was set at 40, 70, and 100 ms to change Td_{scan} while keeping TE constant. The diffusion-gradient duration (δ) was fixed at 7 ms for all experiments. For each Td_{scan}, the b-value was increased from 0 to 8000 s/mm² in 14 steps (0, 2, 250, 500, 750, 1000, 1500, 2000, 3000, 4000, 5000, 6000, 7000, and 8000 s/mm²) by increasing the gradient amplitude. The multi-b-value DWI scan time for each Td_{scan} was 3 min, which means that it took about 10 min for one set of MbMTd DWI. To check scan stability, 5 sets of MbMTd DWI were analyzed in this study.

Model detail: Two-compartment models with inter-compartmental exchange.
The Andrasko-Kärger model is a simple two-compartment model with inter-compartmental compound exchange (Fig. 6, Step 1), and is generally used for pharmacokinetic analyses[15–17]. The water signal ($C(Td)$) from each compartment decreases with a rate constant, q^2D, where q is a spatial frequency determined by the parameters of the motion-probing gradient, and D is the diffusion coefficient of water. The constant t_{ex} represents the lifetime of water molecules in extracellular space before transferring to intracellular space, and t_{in} is the lifetime in the opposite direction. The extracellular and intracellular signals, $C_{ex}(Td)$ and $C_{in}(Td)$ evolve as a function of diffusion-time Td according to the following differential equations,

$$\frac{dC_{ex}(Td)}{dTd} = -\left(q^2 D_{ex} + \frac{1}{t_{ei}}\right)C_{ex}(Td) + \frac{1}{t_{ie}}C_{in}(Td) \tag{4}$$

$$\frac{dC_{in}(Td)}{dTd} = -\left(q^2 D_{in} + \frac{1}{t_{ie}}\right)C_{in}(Td) + \frac{1}{t_{ei}}C_{ex}(Td). \tag{5}$$

D_{ex} and D_{in} are the diffusion coefficients in the extracellular and intracellular spaces, respectively. $C_{ex}(0)$ and $C_{in}(0)$ are equal to the signal fractions of the extracellular (F_{ex}) and intracellular (F_{in}) spaces, respectively (note that $F_{ex} + F_{in} = 1$). Because water exchange from the extra- to intracellular space is equal to that from intra- to extracellular space, F_{ex} and F_{in} are related to the compartment lifetimes as follows:

$$\frac{F_{ex}}{t_{ex}} = \frac{F_{in}}{t_{in}}.$$

(6)

The total DWI signal is the Td-dependent sum of the extra- and intracellular concentrations,

$$\frac{S(Td)}{S_0} = C_{ex}(Td) + C_{in}(Td),$$

(7)

where S0 is the signal for b = 0. After substituting the solutions of Eqs 4 and 5 into Eq. 7

$$\frac{S(Td)}{S_0} = (1 - F_{in}^*)e^{-D_{ex}^* q^2 Td} + F_{in}^* e^{-D_{in}^* q^2 Td},$$

(8)

$$D_{ex}^*, D_{in}^* = \frac{D_{ex} + D_{in} + \frac{\frac{1}{t_{ex}} + \frac{1}{t_{in}}}{q^2} \pm \left(\left[-D_{ex} + D_{in} + \frac{\frac{1}{t_{ex}} + \frac{1}{t_{in}}}{q^2} \right]^2 + \frac{4}{q^4 t_{ex} t_{in}} \right)^{\frac{1}{2}}}{2}$$

(9)

and

$$F_{in}^* = \frac{F_{ex}D_{ex} + F_{in}D_{in} - D_{ex}^*}{D_{in}^* - D_{ex}^*}.$$

(10)

Note that during fitting q^2 is replaced by b/Td_{scan} to accommodate the direct dependence on b-value. Td_{scan} is a constant equal to the Td in each DWI scan. The data observed at each Td_{scan} was fitted to Eq. 8 as a function of b-value.

The model was then modified under the assumption that Td_{scan} is sufficiently long that the diffusion coefficient in the extracellular space (D_{ex}) is approximately constant, while that in the intracellular space (D_{in}) is inversely proportional to the diffusion-time. The data was then analyzed using a Td-independent D_{ex} and α/Td_{scan}^β instead of a constant D_{in}, where β is a parameter inserted to test the assumption that D_{in} is inversely proportional to Td_{scan} ("Modified" in Fig. 2), and the parameter α has dimensions of length squared in the case that $\beta = 1$.

Curve fitting was performed with the nonlinear least-squares method using Matlab (The MathWorks, Inc.). The method "lsqnonlin" in the Optimization Toolbox was used with the algorithm 'trust-region-reflective'.

Data Availability

The datasets analyzed during the current study are available from the corresponding author on reasonable request.

References

1. Chen, S. J. et al. Overactivation of corticotropin-releasing factor receptor type 1 and aquaporin-4 by hypoxia induces cerebral edema. *Proc Natl Acad Sci USA* **111**, 13199–13204, https://doi.org/10.1073/pnas.1404493111 (2014).
2. He, Z. et al. Treadmill pre-training ameliorates brain damage in ischemic stroke via down-regulation of aquaporin-4: an MRI study in rats. *PLoS ONE* **9**, e84602, https://doi.org/10.1371/journal.pone.0084602 (2014).
3. Wang, Y. et al. Regional reproducibility of pulsed arterial spin labeling perfusion imaging at 3T. *Neuroimage* **54**, 1188–1195 (2011).
4. Zeidel, M. L., Ambudkar, S. V., Smith, B. L. & Agre, P. Reconstitution of functional water channels in liposomes containing purified red cell CHIP28 protein. *Biochemistry* **31**, 7436–7440 (1992).
5. Ibata, K., Takimoto, S., Morisaku, T., Miyawaki, A. & Yasui, M. Analysis of aquaporin-mediated diffusional water permeability by coherent anti-stokes Raman scattering microscopy. *Biophys J* **101**, 2277–2283, https://doi.org/10.1016/j.bpj.2011.08.045 (2011).
6. Le Bihan, D. The 'wet mind': water and functional neuroimaging. *Phys Med Biol* **52**, R57–90 (2007).
7. Obata, T. et al. In *ISMRM 20th Annual Scientific Meeting and Exhibition* (1830).
8. Assaf, Y. & Basser, P. J. Composite hindered and restricted model of diffusion (CHARMED) MR imaging of the human brain. *Neuroimage* **27**, 48–58, https://doi.org/10.1016/j.neuroimage.2005.03.042 (2005).
9. Assaf, Y., Freidlin, R. Z., Rohde, G. K. & Basser, P. J. New modeling and experimental framework to characterize hindered and restricted water diffusion in brain white matter. *Magn Reson Med* **52**, 965–978, https://doi.org/10.1002/mrm.20274 (2004).
10. Lam, W. W., Jbabdi, S. & Miller, K. L. A model for extra-axonal diffusion spectra with frequency-dependent restriction. *Magn Reson Med*, https://doi.org/10.1002/mrm.25363 (2014).
11. Thelwall, P. E., Grant, S. C., Stanisz, G. J. & Blackband, S. J. Human erythrocyte ghosts: exploring the origins of multiexponential water diffusion in a model biological tissue with magnetic resonance. *Magn Reson Med* **48**, 649–657, https://doi.org/10.1002/mrm.10270 (2002).
12. Thelwall, P. E., Shepherd, T. M., Stanisz, G. J. & Blackband, S. J. Effects of temperature and aldehyde fixation on tissue water diffusion properties, studied in an erythrocyte ghost tissue model. *Magn Reson Med* **56**, 282–289, https://doi.org/10.1002/mrm.20962 (2006).
13. Li, H. et al. Time-Dependent Influence of Cell Membrane Permeability on MR Diffusion Measurements. *Magn Reson Med* **75**, 1927–1934, https://doi.org/10.1002/mrm.25724 (2016).
14. Fieremans, E., Novikov, D. S., Jensen, J. H. & Helpern, J. A. Monte Carlo study of a two-compartment exchange model of diffusion. *NMR in biomedicine* **23**, 711–724 (2010).
15. Lee, J.-H. & Springer, C. S. Jr. Effects of equilibrium exchange on diffusion-weighted NMR signals: the diffusigraphic "shutter-speed". *Magn Reson Med* **49**, 450–458 (2003).

16. Andrasko, J. Water diffusion permeability of human erythrocytes studied by a pulsed gradient NMR technique. *Biochim Biophys Acta* **428**, 304–311 (1976).
17. Kaerger, J., Pfeifer, H. & Heink, W. Principles and application of self-diffusion measurements by nuclear magnetic resonance. *Adv Magn Reson* **12**, 1–89 (1988).
18. Callaghan, P. T. In *Translational Dynamics and Magnetic Resonance, Principles of Pulsed Gradient Spin Echo NMR* 312–316 (Oxford University Press, 2011).
19. Sen, P. N. Time-dependent diffusion coefficient as a probe of geometry. *Concepts in Magnetic Resonance Part A* **23a**, 1–21 (2004).
20. Dmytrenko, L. *et al*. The impact of alpha-syntrophin deletion on the changes in tissue structure and extracellular diffusion associated with cell swelling under physiological and pathological conditions. *PLoS ONE* **8**, e68044, https://doi.org/10.1371/journal.pone.0068044 (2013).
21. Clark, C. A. & Le Bihan, D. Water diffusion compartmentation and anisotropy at high b values in the human brain. *Magn Reson Med* **44**, 852–859 (2000).
22. Callaghan, P. T. In *Principles of Nuclear Magnetic Resonance Microscopy* 371–399 (Clarendon Press, 1991).
23. Duplay, R. & Sen, P. N. Influence of local geometry and transition to dispersive regime by mechanical mixing in porous media. *Phys Rev E Stat Nonlin Soft Matter Phys* **70**, 066309 (2004).
24. Tachibana, A. *et al*. Comparison of Glass Capillary Plates and Polyethylene Fiber Bundles as Phantoms to Assess the Quality of Diffusion Tensor Imaging. *Magn Reson Med Sci*, https://doi.org/10.2463/mrms.mp.2017-0079 (2017).
25. Obata, T. *et al*. In *ISMRM 24th Annual Scientific Meeting and Exhibition* (2010).
26. Lemberskiy, G. *et al*. Time-Dependent Diffusion in Prostate Cancer. *Invest Radiol* **52**, 405–411, https://doi.org/10.1097/RLI.0000000000000356 (2017).
27. Latt, J. *et al*. Diffusion-weighted MRI measurements on stroke patients reveal water-exchange mechanisms in sub-acute ischaemic lesions. *NMR Biomed* **22**, 619–628, https://doi.org/10.1002/nbm.1376 (2009).
28. Nilsson, M. *et al*. Noninvasive mapping of water diffusional exchange in the human brain using filter-exchange imaging. *Magn Reson Med* **69**, 1573–1581, https://doi.org/10.1002/mrm.24395 (2013).
29. Lundell, H., Alexander, D. C. & Dyrby, T. B. High angular resolution diffusion imaging with stimulated echoes: compensation and correction in experiment design and analysis. *NMR Biomed* **27**, 918–925, https://doi.org/10.1002/nbm.3137 (2014).
30. Ozarslan, E. *et al*. Observation of anomalous diffusion in excised tissue by characterizing the diffusion-time dependence of the MR signal. *J Magn Reson* **183**, 315–323, https://doi.org/10.1016/j.jmr.2006.08.009 (2006).
31. Verkman, A. S., Anderson, M. O. & Papadopoulos, M. C. Aquaporins: important but elusive drug targets. *Nature reviews. Drug discovery* **13**, 259–277, https://doi.org/10.1038/nrd4226 (2014).
32. Bonfrate, L., Procino, G., Wang, D. Q., Svelto, M. & Portincasa, P. A novel therapeutic effect of statins on nephrogenic diabetes insipidus. *Journal of cellular and molecular medicine* **19**, 265–282, https://doi.org/10.1111/jcmm.12422 (2015).
33. Kang, B. W. *et al*. Expression of aquaporin-1, aquaporin-3, and aquaporin-5 correlates with nodal metastasis in colon cancer. *Oncology* **88**, 369–376, https://doi.org/10.1159/000369073 (2015).
34. Zhong, J. H., Gore, J. C. & Armitage, I. M. Relative contributions of chemical exchange and other relaxation mechanisms in protein solutions and tissues. *Magn Reson Med* **11**, 295–308 (1989).
35. Wheatley, D. N., Rimmington, J. E. & Foster, M. A. Effects of osmotic manipulation of intracellular hydration of HeLa S-3 cells on their proton NMR relaxation times. *Magn Reson Imaging* **8**, 285–293 (1990).
36. Lester, C. C. & Bryant, R. G. Water-proton nuclear magnetic relaxation in heterogeneous systems: hydrated lysozyme results. *Magn Reson Med* **22**, 143–153 (1991).
37. Roth, Y. *et al*. Quantification of water compartmentation in cell suspensions by diffusion-weighted and T(2)-weighted MRI. *Magn Reson Imaging* **26**, 88–102 (2008).
38. Fieremans, E. *et al*. *In vivo* measurement of membrane permeability and myofiber size in human muscle using time-dependent diffusion tensor imaging and the random permeable barrier model. *NMR Biomed* **30**, https://doi.org/10.1002/nbm.3612 (2017).
39. Koay, C. G., Ozarslan, E. & Basser, P. J. A signal transformational framework for breaking the noise floor and its applications in MRI. *J Magn Reson* **197**, 108–119, https://doi.org/10.1016/j.jmr.2008.11.015 (2009).
40. Ozarslan, E., Shepherd, T. M., Koay, C. G., Blackband, S. J. & Basser, P. J. Temporal scaling characteristics of diffusion as a new MRI contrast: findings in rat hippocampus. *Neuroimage* **60**, 1380–1393, https://doi.org/10.1016/j.neuroimage.2012.01.105 (2012).
41. Miyazaki, K. *et al*. Establishment of monoclonal antibodies against the extracellular domain that block binding of NMO-IgG to AQP4. *Journal of neuroimmunology* **260**, 107–116, https://doi.org/10.1016/j.jneuroim.2013.03.003 (2013).
42. Kato, Y. *et al*. Unprecedented cell-selection using ultra-quick freezing combined with aquaporin expression. *PLoS ONE* **9**, e87644, https://doi.org/10.1371/journal.pone.0087644 (2014).

Acknowledgements

Author Contributions

T.O. designed the study, performed the experiments, analyzed the data and wrote the manuscript. J.K. performed the experiments, analyzed the data and wrote the manuscript. Y.T. analyzed the data and wrote the manuscript. T.M. performed the experiments, analyzed the data and wrote the manuscript. Y.A. performed the experiments and wrote the manuscript. S.S. performed the experiments and analyzed the data. H.K. analyzed the data. Y.I. analyzed the data. H.T. performed the experiments. I.A. performed the experiments and wrote the manuscript. M.Y. performed the experiments, analyzed the data and wrote the manuscript.

Additional Information

Supplementary information accompanies this paper at https://doi.org/10.1038/s41598-018-36264-9.

Competing Interests: The authors declare no competing interests.

Publisher's note: Springer Nature remains neutral with regard to jurisdictional claims in published maps and institutional affiliations.